

# Echo State Network for Features Extraction and Segmentation of Tomography Images\*

Petia Koprinkova-Hristova<sup>1</sup>, Ivan Georgiev<sup>1,2</sup>, Miryana Raykovska<sup>1</sup>

<sup>1</sup> Institute of Information and Communication technologies, Bulgarian Academy of Sciences  
Acad. G. Bonchev str. bl.2, Sofia 1113, Bulgaria

petia.koprinkova@iict.bas.bg  
ivan.georgiev@parallel.bas.bg  
miriana.raykovska@iict.bas.bg

<sup>2</sup> Institute of Mathematics and Informatics, Bulgarian Academy of Sciences  
Acad. G. Bonchev str. bl.8, Sofia 1113, Bulgaria

**Abstract.** The paper proposes a novel approach for gray scale images segmentation. It is based on multiple features extraction from a single feature per image pixel, namely its intensity value, via a recurrent neural network from the reservoir computing family - Echo state network. The preliminary tests on the benchmark gray scale image Lena demonstrated that the newly extracted features - reservoir equilibrium states - reveal hidden image characteristics. In present work the developed approach was applied to a real life task for segmentation of a 3D tomography image of a of bone whose aim was to explore the object's internal structure. The achieved results demonstrated the novel approach allows for clearer revealing the details of the bone internal structure thus supporting further tomography image analyses.

**Keywords:** reservoir computing, Echo state network, intrinsic plasticity, gray image, segmentation, tomography.

## 1. Introduction

Image segmentation aims division of a digital image into segments in order to reduce its complexity and thus to enable further processing or analysis. It has many practical applications including medical image analysis, computer vision for autonomous vehicles, face recognition and detection, video surveillance, satellite image analysis etc.

Image segmentation is done by assignment of labels to pixels in dependence on their belonging to individual objects in the image, such as people, animals, flowers, cars etc. Usually high-level features such as color or contrast are applied by the traditional approaches. However, these have to be fine tuned or manually assigned so the obtained results might not be accurate enough, especially for complex images.

Modern segmentation techniques relay on machine learning approaches, such as deep learning neural networks [29], for automated features extraction and segmentation. In case of gray images such as produced for medical diagnostics Computed Tomography (CT), Magnetic Resonance Imaging (MRI) etc., the problem for clearer separation of regions of interest is of crucial importance because they were often used for tumor detection or

---

\* This is an extended version of the conference paper "Reservoir Computing Approach for Gray Images Segmentation", presented at IEEE INISTA 2022.

diagnostic of brain deceases. A recent review in the area [26] concludes that all of the applied by far algorithms need broad improvement. Extensive research on gray and/or medical images includes numerous approaches such as heuristic optimization algorithms like bee colony [6] or Particle swarm [1], artificial neural networks [23, 22, 19] including deep ones [15, 14, 9, 30, 5, 25, 4, 2], gray value thresholding [21], Gaussian mixture models [18], Support vector machines [3], neuro-fuzzy approaches [24, 8] etc.

However, the most often applied DNNs need huge amount of training examples as well as big computational resources and time to be trained properly. In contrast to them Echo state networks (ESN) belong to a novel and rapidly developing family of reservoir computing approaches [7, 17] whose primary aim was development of fast trainable recurrent neural network architectures (RNN) for approximation of nonlinear time series. Following different view point to dynamic reservoir structure and its properties, in [10] a novel approach for features extraction from multidimensional data sets using ESN was proposed. It was successfully tested on numerous practical examples, among which clustering and segmentation of multi-spectral images [11].

The core of the original approach was to use the reservoir equilibrium states corresponding to each one of multidimensional input data. The fitting of the ESN reservoir dynamics to reflect the input data structure was achieved using an approach for tuning of ESN reservoir internal connectivity and dynamics called Intrinsic Plasticity (IP) [28, 27].

In [13] a modified version of the approach from [11] for segmentation of gray scale images was proposed. In order to enhance original gray image an IP tuned ESN reservoir was applied to extract multiple features from the intensity value of each pixel that are reservoir neurons equilibrium states corresponding to the pixels' intensities. The extracted features were further used by a segmentation routine to divide image into several segments (clusters). Comparison of segmentation results on the benchmark gray image Lena revealed that using the extracted via ESN features and kmeans clustering allowed to reveal hidden image details in comparison with clustering via the scalar original feature (image pixel intensity).

The present work continues investigation of our newly proposed approach applying it to a real life problem - 3D micro-CT tomography image purification via segmentation.

The paper is organized as follows: the next section 2 introduces ESN, IP tuning algorithm and adapted to gray scale images approach for features extraction; the following section presents obtained results on a set of tomography images collection; the paper finishes with concluding remarks and direction for future work.

## 2. ESN Approach for Gray Scale Images Features Extraction

### 2.1. ESN and IP tuning

The structure of an ESN is shown on Fig 1.

It incorporates a dynamic reservoir of neurons with a sigmoid activation function  $f^{res}$  (usually the hyperbolic tangent) and randomly generated recurrent connections  $W^{res}$ . The reservoir state for the current time instant  $k$   $r(k)$  depends both on its previous state  $r(k-1)$  and on the current input  $u(k)$  as follows:

$$r(k) = f^{res}(diag(a)W^{in}u(k) + W^{res}r(k-1) + diag(b)) \quad (1)$$

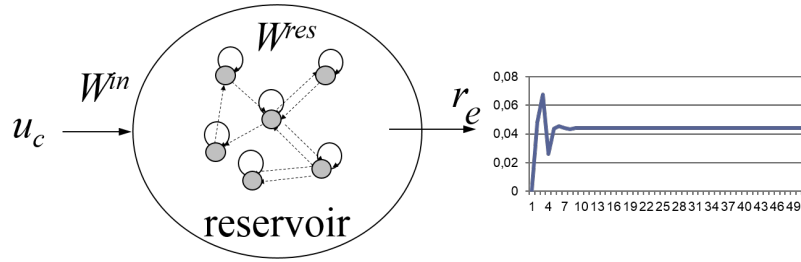


**Fig. 1.** ESN for features extraction

Here  $W^{in}$  and  $W^{res}$  are input and recurrent connection weight matrices that are randomly generated according to recipes given by [17];  $a$  and  $b$  are vectors called gain and bias that are set to 1 and 0 respectively in most applications. For the aim of time series modelling the readout of reservoir is a linear combination of its current state whose parameters are the only trainable parameters of this recurrent neural network structure. However, in present investigation as in [10] we will focus only on characteristics of the reservoir equilibrium state  $r_e$  achieved after feeding of constant input  $u_c$  until the reservoir settles down (as shown on Fig. 1).

In order to adjust the reservoir to the structure of its input data, [28, 27] proposed an approach called Intrinsic Plasticity (IP) tuning that achieves desired distribution of reservoir output via changes in the gain  $a$  and bias  $b$  in equation (1). The procedure is gradient algorithm minimizing Kullback-Leibler divergence between actual and target distributions. In case of hyperbolic tangent activation function the proper target distribution is normal (Gaussian) with mean  $\mu$  and variance  $\sigma$ :

$$p_{norm} = (1/\sigma\sqrt{2\pi})e^{-(r-\mu)^2/2\sigma^2} \tag{2}$$

Thus the training rules for IP tuning of gain and bias vectors derived in [27] are:

$$\Delta b = -\eta(-\mu/\sigma^2 + r/\sigma^2(2\sigma^2 + 1 - r^2 + \mu r)) \tag{3}$$

$$\Delta a = \eta/a + \Delta b x \tag{4}$$

Here  $\eta$  is learning rate and  $x = W^{in}u + W^{res}r$  is the net input to the reservoir neurons. The Algorithm 1 presents the IP tuning procedure. All original data vectors (in our terminology further features)  $f(i), i = 1 \div n_f$  are fed consecutively to the ESN reservoir with zero initial state  $r(0) = 0$  for  $n_{IP}$  IP tuning iterations (usually 3-5 are enough as in [27]).

In [10] for the first time it was proposed to exploit the achieved by feeding of multidimensional data input equilibrium states of IP tuned ESN reservoir as new feature vector. In [11] the approach was applied to various multidimensional data sets for the aims of clustering. It was demonstrated that projections onto new (ESN equilibrium) state space could led to better data separation. The Algorithm 2 present the features extraction procedure.

**Algorithm 1** IP tuning

---

*IP tuning of ESN*

2: Generate initial ESN reservoir  
 $r(0) = 0$

4:  $a(0) = 1$   
 $b(0) = 0$

6: **for**  $k = 1 \div n_{IP}$  **do**  
  **for**  $i = 1 \div n_f$  **do**  
8:    $x(i) = W^{in}f(i) + W^{res}r(i-1)$   
    $r(i) = \tanh(a(i-1)x(i) + b(i-1))$   
10:    $a(i) = a(i-1) + \Delta a(i)$   
    $b(i) = b(i-1) + \Delta b(i)$   
12:   **end for**  
**end for**

---

**Algorithm 2** Features extraction

---

*Extract features from IP tuned ESN*

2: **for**  $i = 1 \div n_f$  **do**  
   $r(0) = 0$   
4:   **for**  $k = 1 \div n_{it}$  **do**  
    $x(k) = W^{in}f(i) + W^{res}r(k-1)$   
6:    $r(k) = \tanh(ax(k) + b)$   
   **end for**  
8:    $r_e^i = r(k)$   
**end for**

---

All original vectors of features  $f(i), i = 1 \div n_f$  are fed consecutively  $n_{it}$  times as constant input  $u(k) = f(i) = const., k = 1 \div n_{it}$  to the ESN reservoir with zero initial state  $r(0) = 0$  until it settles to a new equilibrium state  $r_e(f(i)) = r(n_{it})$ .  $n_{it}$  is number of iterations needed to achieve steady state  $r_e = r(k) = r(k-1)$  of the reservoir. Achieved in this way equilibrium states of the ESN reservoir  $r_e^i$  for each original features vector  $f(i)$  are considered as new features.

**2.2. Approach for features extraction from gray scale images**

In [10] it was investigated how the IP tuning of a randomly generated ESN reservoir led to clearer separation of the original multidimensional data after its projection to low dimensional space. The effect of IP tuning on reservoir equilibrium state was further investigated in [12] demonstrating that it increases equilibrium states memory capacity and is strongly influenced by the original data structure. Provoked by the needs of gray scale images clustering, in [13] a modification of the original approach for features extraction was proposed. In contrast to [10], from each single feature per pixel (that is its intensity value  $f(i) = pi(i), i = 1 \div n_{pi}$ ) multiple features corresponding to ESN reservoir neurons equilibrium states  $r_e^i$  were obtained ( $n_f = n_{pi}$  is the number of the gray image pixels;  $pi(i)$  is  $i$ -th pixel intensity). Thus feeding of pixel by pixel intensities of an original gray image to the IP tuned ESN reservoir yields multiple filtered images as shown on Fig. 2. The obtained in this way multidimensional feature vector per pixel are subject to

clustering via kmeans using one selected feature among numerous extracted once or all of them.

### 3. Results and Discussion

In [13] the proposed approach was tested on the gray version of the benchmark image Lena. In present work a real life problem - 3D micro-CT tomography image purification via segmentation - was considered. Here we briefly present the results from [13] first and then continue with tomography data.

#### 3.1. Lena Segmentation

In order to investigate effects of proposed features extraction approach a benchmark image Lena was used. The original colour image was converted to gray scale and pixels intensities  $pi$  were scaled in range  $[-1, 1]$ . Next, all pixels intensities were applied to tune the gain and bias parameters of a randomly generated fully connected ESN reservoir with size  $n_r = 10$  and spectral radius 0.9. The target Gaussian distribution of IP tuning was with zero mean and variance  $\sigma = 0.1$  and number of IP tuning iterations was set to  $n_{IP} = 5$ . The number of iterations needed to achieve reservoir steady state was estimated to  $n_{it} = 50$ .

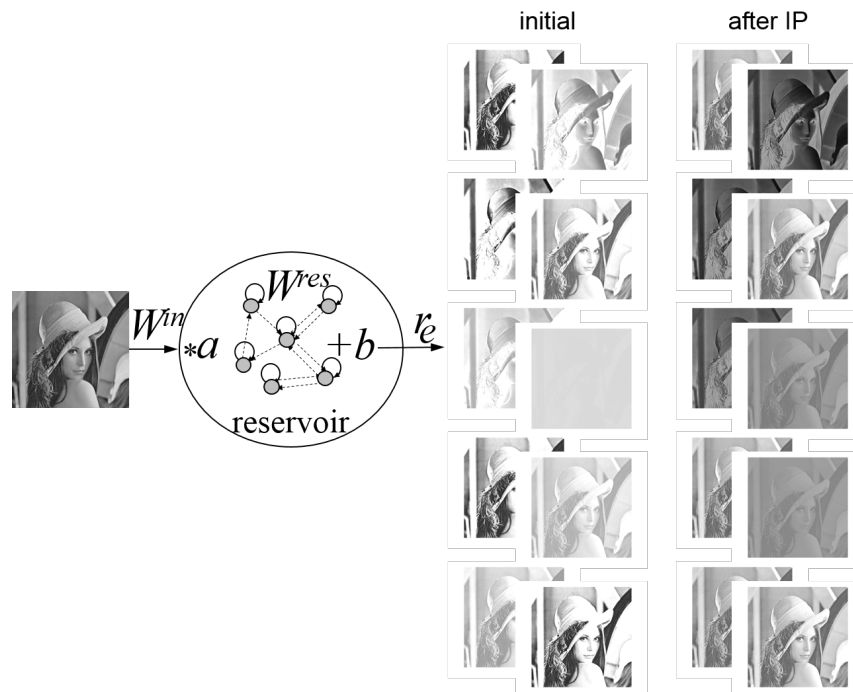


**Fig. 2.** Gray image features extraction

For the seek of comparison features were extracted by initial and IP tuned reservoir as shown on Fig. 2. Fig. 3 shows histograms of the original image pixels intensities vs the histograms of features extracted by initial and IP tuned ESN reservoirs.

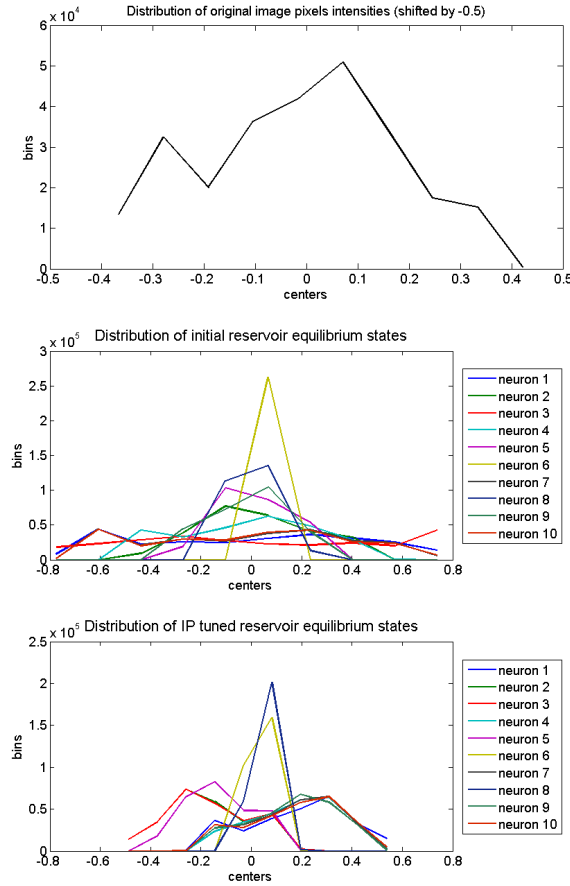


**Fig. 3.** Histogram of the original image pixels intensities shifted by  $-0.5$  (top) vs the equilibrium states distributions of the initial (middle) and IP tuned reservoir (bottom)

The observed effects of IP tuning are following: the reservoir equilibrium states were squeezed in narrow interval; the distribution of new equilibrium states reflects the original data distribution.

Next kmeans clustering algorithm was applied to separate image pixels into clusters using all original and all extracted by initial and IP tuned reservoir features. From Fig. 3 is clear that features extracted from IP tuned reservoir can be visually separated into three groups - having maximum around  $-0.3$ ,  $0.1$  and  $0.3$  respectively that is in accordance other segmentation approaches tested on Lena image. So the number of clusters was set

to three here. The representative features from the three groups in Fig. 3 (neurons 1, 3 and 8) were selected for clustering too.

Comparison of the original gray image and its segmentation via kmeans clustering are shown in Fig. 4. While segmentation using features extracted by initial random ESN reservoir looks blurred, the results achieved using IP tuned reservoir reveal sharper discrimination between image regions. Segmentation via representative features (neurons 1, 3 and 8) seems quite similar to that achieved using all features extracted by IP tuned reservoir. Looking at Fig. 4, it is observed that the results achieved using features extracted by IP tuned reservoir look quite similar to those obtained by kmeans clustering of original image pixels intensities. However, IP tuned reservoir features revealed a little bit more details from the original image, e.g. some light bunches in the hair, shades on the shoulder, contours in the background stuff etc.



**Fig. 4.** Segmentation of the original gray image on the top into three clusters by kmeans clustering, from left to right using all features extracted by the initial reservoir, by all features extracted from the IP tuned reservoir and by the features from the representative neurons 1, 3 and 8

Comparison between results before and after IP tuning shows that fitting the reservoir to the input data allows to achieve sharper discrimination between regions with different grades of pixels intensities. Besides, in [13] it was observed that each neuron acts as a filter revealing different image characteristics.



**Fig. 5.** Segmentation of the original gray image into three clusters using original image pixels intensities, from left to right via hard thresholding, multi-level thresholding, fuzzy c-means, subtractive clustering and kmeans clustering

For the seek of comparison the gray image was segmented using original pixels intensities and several clustering approaches: kmeans, hard thresholding using fixed threshold levels equally distributed within range of pixels intensities, multi-level thresholding using Otsu's method [20], fuzzy c-means clustering and subtractive clustering [31]. Fig. 5 presents comparison of the original gray image and its segmentation by enumerated clustering approaches. It is obvious that kmeans segmentation outperforms all other approaches achieving sharper segmentation of the image.

### 3.2. Tomography Image Segmentation

The sample was scanned through a micro-CT device Nikon XT H 225. The X-ray parameters were a voltage of 100 kV and a current of 100  $\mu$ A. A Series of 2000 projections with one frame per projection, an exposure time of 500 ms, and an isotropic resolution of 97  $\mu$ m per voxel were acquired during a continuous rotation range of 360°. The images were reconstructed with CT Pro 3D (version XT 3.1.3, Nikon Metrology, Hertfordshire, UK), using a beam hardening correction and noise reduction and a median filter with a kernel size of 3X3. ROI of interest was selected and extracted as a separate volume from a human skull's central part of the sutura sagittalis.

In order to determine proper number of clusters kmeans clustering was applied to a single slice of the original tomography image. Results from segmentation into two, three and four classes are shown on Fig. 6. It is obvious that the higher the number of clusters is the more details from the gray image are discovered via segmentation.

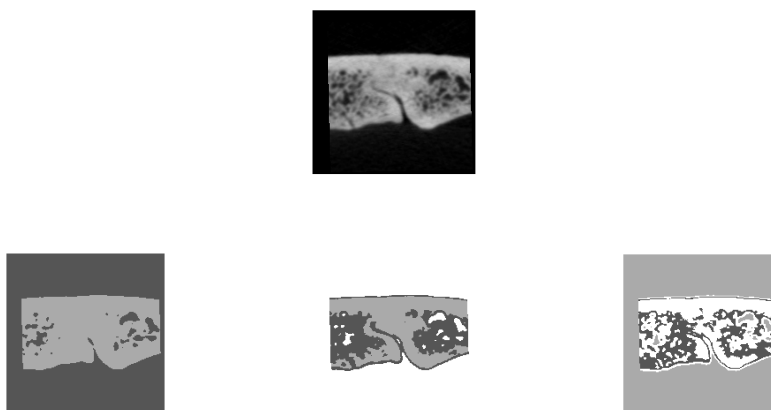


**Fig. 6.** Segmentation of the original image (top) into two (bottom, left), three (bottom, middle) and four (bottom, right) clusters

In order to assess the segmentation quality clusters silhouettes are compared on Fig. 7. Although the segmentation into four clusters seems more impressive on Fig. 6, its maximal silhouette value (0.9906) is slightly lower than that in the three clusters case

(0.9912). In case of two clusters the maximal silhouette value (0.9886) is the smallest one. Thus the proper number of clusters is two.

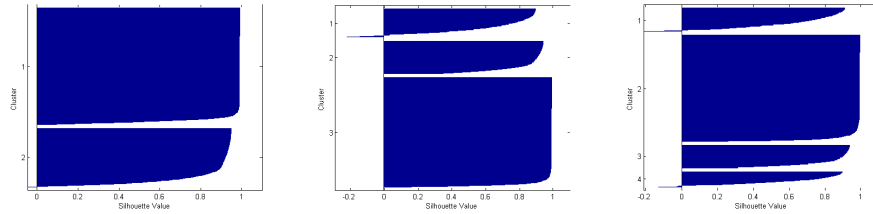


**Fig. 7.** Silhouettes of clusters in case of two (left), three (middle) and four (right) classes respectively

The initial random ESN reservoir with the same parameters as in previous example was IP tuned using a single slice from a different tomography collection. Next the IP tuned reservoir was applied to extract features of the investigated tomography image. Next kmeans clustering into two classes was applied using all ESN extracted multidimensional features as well as on each ESN feature separately. For the seek of comparison kmeans clustering was applied to the original image using points gray scale as a feature.

In order to asses segmentation results without ground truth information several approaches are applied [32]. Here we compare the squared error (Fig. 8) and the average squared error of the segments  $F(I)$  (Fig. 9) as in [16].

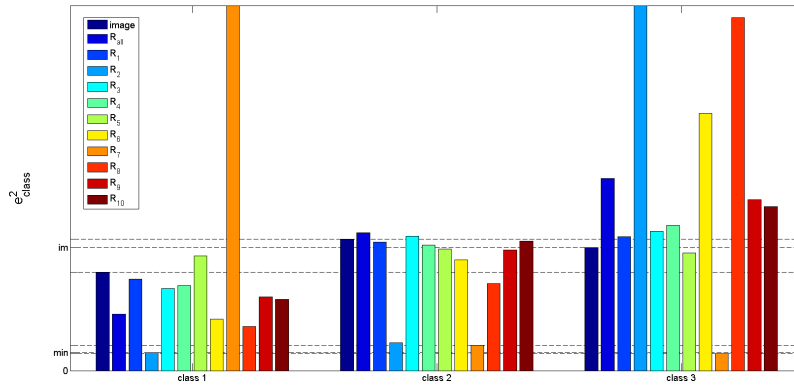


**Fig. 8.** Squared error per cluster

Fig. 8 reveals that using all ESN extracted features does not outperform segmentation from the original image features. However, several single ESN features give much better results for some of the segments, e.g.  $R7$  that is the steady state of neuron number 7 of

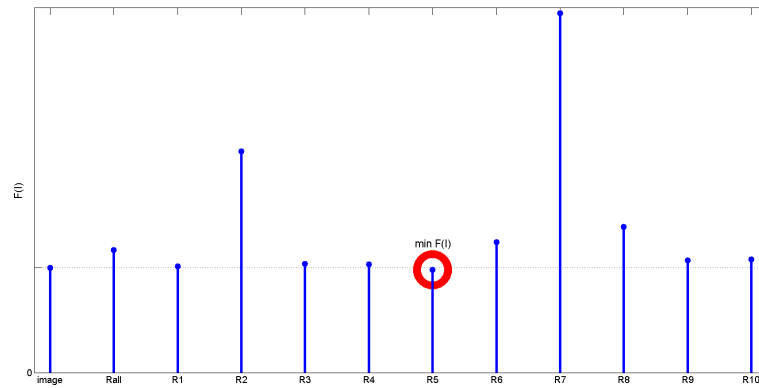


**Fig. 9.** Average squared error of all clusters

the ESN reservoir achieves the lowest error for classes 2 and 3 but the worst result for class 1. Fig. 9 shows that the average squared error  $F(I)$  is lowest in case of feature  $R5$ . However, visual assessment of the segmentation results does not support this quantitative conclusion.

Fig. 10 shows entropy-based evaluation metric from [33]. It reveals that feature  $R7$  is the best one based on this measure.

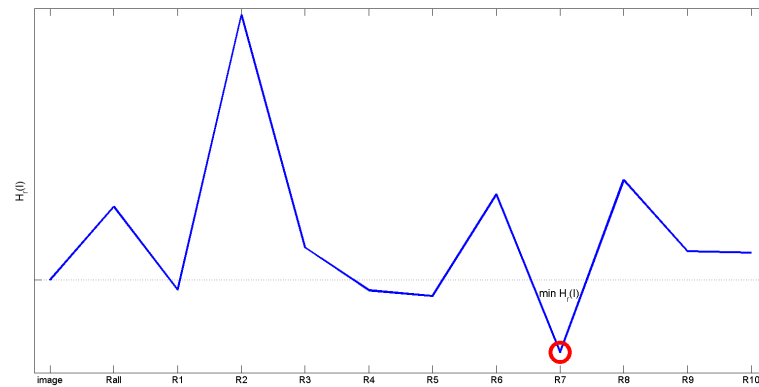


**Fig. 10.** Entropy evaluation metric

Fig. 11 shows the original unsegmented render (3D tomography image) and its segmentation into three classes using original features (pixels intensities) as well ESN ex-

tracted features. As expected, clustering made the image less blurred. The best segmentation was achieved by a single ESN extracted feature (from neuron 7).

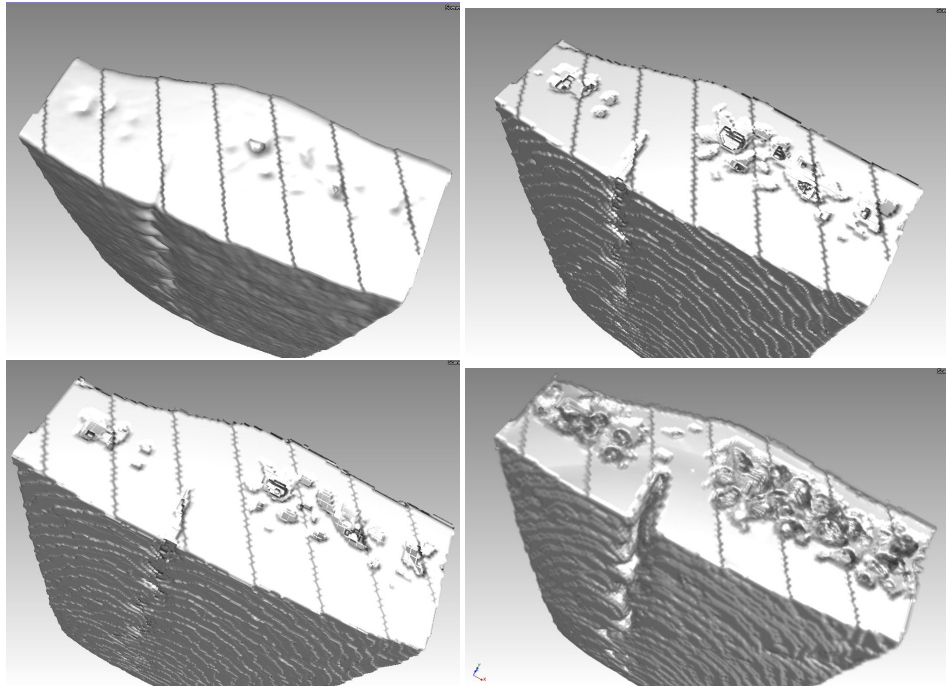


**Fig. 11.** Original tomography image (top, left) versus segmentation into three clusters via original image pixels intensities (top, right), all ESN extracted features (bottom, left) and best extracted feature from neuron 7 (bottom, right)

In order to explore the deeper structure of the investigated bone sample we show two representative vertical and horizontal 2D slices from the 3D image as shown on Fig. 12. Figure 13 shows the representative slices on horizontal and vertical directions from the original tomography image while at Fig. 12 while figures 14, 15 and 16 show the corresponding representative 2D slices from the segmented 3D images using original pixels intensities, all and the best ESN extracted features respectively.

While results achieved using original and all ESN extracted features look similar, the clustering via the best ESN feature reveals much more details of the tomography image. In it the compact and spongy layers of the bone are most clearly distinguished and the bone suture is fully visible in terms of placement and shape. The most impressive result is the clearest visualization of the skull seam.

#### 4. Conclusions

Our results demonstrated that using of IP tuned ESN for features extraction from the tomography images gives numerous features among which the best ones revealed hidden

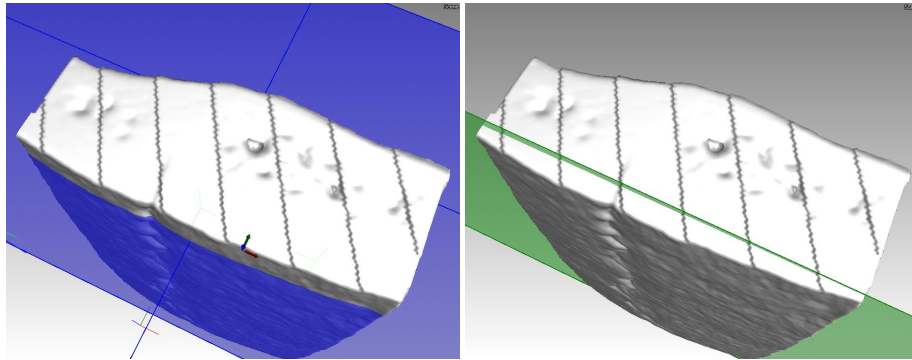


**Fig. 12.** Representative horizontal (blue plane) and vertical (green plane) 2D slices positions

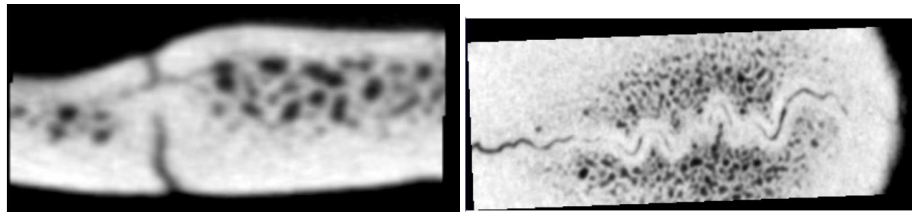


**Fig. 13.** 2D slices from the original tomography image

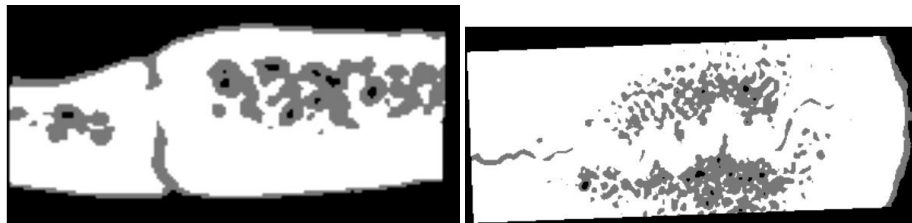


**Fig. 14.** 2D slices from the segmented via original tomography image pixels intensities



**Fig. 15.** 2D slices from the segmented tomography image via all ESN extracted features

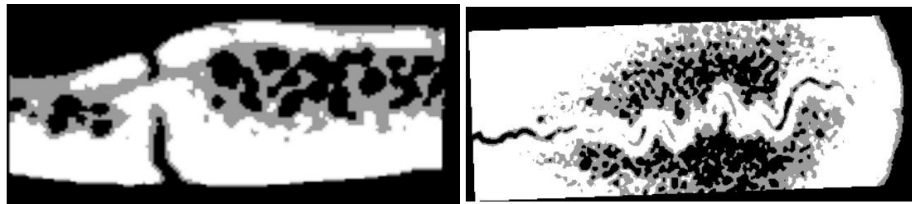


**Fig. 16.** 2D slices from the segmented tomography image via the best single ESN extracted feature

image details. Clustering results based on a chosen best extracted feature demonstrated impressively better segmentation of the gray image in comparison with the segmentation by its original pixels intensity.

These preliminary results are good basis for further development of hierarchical (deep) approach for gray images segmentation combining ESN and clustering approaches.

**Acknowledgments.** We acknowledge the provided access to the e-infrastructure of the Laboratory for 3D Digitization and Microstructure Analysis at IICT-BAS, Grant No BG05M2OP001-1.001-0003. The second author was partially supported by the Bulgarian NSF Grant KP-06-N27/6. The third author was partially supported by the Bulgarian NSF Grant KP-06-N53/7.

## References

1. Alraddady, F., Zanaty, E.A., Abu bakr, A.H., Abd-Elhafiez, W.M., Fusion Strategy for Improving Medical Image Segmentation (2023) *Computers, Materials and Continua*, 74 (2), pp. 3627-3646.
2. Arutperumjothi, G., Devi, K.S., Rani, C., Srinivasan, P., Qualitative Abnormalities of Peripheral Blood Smear Images Using Deep Learning Techniques (2023) *Intelligent Automation and Soft Computing*, 35 (1), pp. 1069-1086.
3. Bao, X.-X., Zhao, C., Bao, S.-S., Rao, J.-S., Yang, Z.-Y., Li, X.-G., Recognition of necrotic regions in MRI images of chronic spinal cord injury based on superpixel (2023) *Computer Methods and Programs in Biomedicine*, 228, art. no. 107252.
4. Fang, L., Wang, X., Multi-input Unet model based on the integrated block and the aggregation connection for MRI brain tumor segmentation (2023) *Biomedical Signal Processing and Control*, 79, art. no. 104027.
5. Huang, X., Liu, Y., Li, Y., Qi, K., Gao, A., Zheng, B., Liang, D., Long, X., Deep Learning-Based Multiclass Brain Tissue Segmentation in Fetal MRIs (2023) *Sensors*, 23 (2), art. no. 655.
6. Ibrahim, S., Abu Samah, K.A.F., Hamzah, R., Ali, N.A.M., Aminuddin, R., Substantial adaptive artificial bee colony algorithm implementation for glioblastoma detection (2023) *IAES International Journal of Artificial Intelligence*, 12 (1), pp. 443-450.
7. Jaeger, H., Tutorial on training recurrent neural networks, covering BPPT, RTRL, EKF and the "echo state network" approach. GMD Report 159, German National Research Center for Information Technology (2002)
8. Karthikeyan, M.P., Mary Anita, E.A., IM-EDRD from Retinal Fundus Images Using Multi-Level Classification Techniques (2023) *Intelligent Automation and Soft Computing*, 35 (1), pp. 567-580.

9. Khan, R., Akbar, S., Mehmood, A., Shahid, F., Munir, K., Ilyas, N., Asif, M., Zheng, Z., A transfer learning approach for multiclass classification of Alzheimer's disease using MRI images (2023) *Frontiers in Neuroscience*, 16, art. no. 1050777.
10. Koprinkova-Hristova, P., Tontchev, N., Echo state networks for multidimensional data clustering, In: Villa, A.E.P., Duch, W., Érdi, P., Masulli, F., Palm, G. (eds.) *Int. Conf. on Artificial Neural Networks 2012*, LNCS vol. 7552, pp. 571–578. Springer, Heidelberg (2012)
11. Koprinkova-Hristova, P., Multidimensional data clustering and visualization via Echo state networks, In: Kountchev, R., Nakamatsu, K. (eds.) *New Approaches in Intelligent Image Analysis*, Intelligent Systems Reference Library vol. 108, pp. 93–122. Springer, Cham (2016)
12. Koprinkova-Hristova, P., On effects of IP improvement of ESN reservoirs for reflecting of data structure. In: *Proc. of the International Joint Conference on Neural Networks (IJCNN) 2015*, IEEE, Killarney, Ireland, DOI: 10.1109/IJCNN.2015.7280703 (2015)
13. Koprinkova-Hristova, P., Reservoir computing approach for gray images segmentation. In: *Proc. of the 2022 International Conference on INnovations in Intelligent SysTems and Applications (INISTA) 2022*, pp. 1-6, DOI: 10.1109/INISTA55318.2022.9894221 (2022)
14. Lee, J., Lee, M., Lee, J., Kim, R.E.Y., Lim, S.H., Kim, D., Fine-grained brain tissue segmentation for brain modeling of stroke patient (2023) *Computers in Biology and Medicine*, 153, art. no. 106472.
15. Lin, C.-T., Ghosh, S., Hinkley, L.B., Dale, C.L., Souza, A.C.S., Sabes, J.H., Hess, C.P., Adams, M.E., Cheung, S.W., Nagarajan, S.S., Multi-tasking deep network for tinnitus classification and severity prediction from multimodal structural MR images (2023) *Journal of Neural Engineering*, 20 (1), art. no. 016017.
16. Liu, J., Yang, Y.-H., Multi-resolution color image segmentation, *IEEE Transactions on Pattern Analysis and Machine Intelligence*, vol. 16 (7), 1994, pp. 689–700.
17. Lukosevicius, M., Jaeger, H., Reservoir computing approaches to recurrent neural network training, *Computer Science Review*, vol. 3, pp. 127–149 (2009)
18. Mamalakis, M., Garg, P., Nelson, T., Lee, J., Swift, A.J., Wild, J.M., Clayton, R.H., Automatic development of 3D anatomical models of border zone and core scar regions in the left ventricle (2023) *Computerized Medical Imaging and Graphics*, 103, art. no. 102152.
19. Mustafa, S., Jaffar, A., Iqbal, M.W., Abubakar, A., Alshahrani, A.S., Alghamdi, A., Hybrid Color Texture Features Classification Through ANN for Melanoma (2023) *Intelligent Automation and Soft Computing*, 35 (2), pp. 2205-2218.
20. Otsu, N., A threshold selection method from gray-level histograms, *IEEE Trans. on SMC*, vol. 9 (1), 1979, pp.62-66.
21. Palmkron, S.B., Bergenståhl, B., Håkansson, S., Wahlgren, M., Fureby, A.M., Larsson, E., Quantification of structures in freeze-dried materials using X-ray microtomography (2023) *Colloids and Surfaces A: Physicochemical and Engineering Aspects*, 658, art. no. 130726.
22. Pavuluri, K., Scott, J.M., Huston III, J., Ehman, R.L., Manduca, A., Jack Jr, C.R., Savica, R., Boeve, B.F., Kantarci, K., Petersen, R.C., Knopman, D.S., Murphy, M.C., Differential effect of dementia etiology on cortical stiffness as assessed by MR elastography (2023) *NeuroImage: Clinical*, 37, art. no. 103328.
23. Putri, E.R., Zarkasi, A., Prajitno, P., Soejoko, D.S., Artificial neural network for cervical abnormalities detection on computed tomography images (2023) *IAES International Journal of Artificial Intelligence*, 12 (1), pp. 171-179.
24. Rahman, J.S.U., Selvaperumal, S.K., Integrated approach of brain segmentation using neuro fuzzy k-means (2023) *Indonesian Journal of Electrical Engineering and Computer Science*, 29 (1), pp. 270-276.
25. Rajagopal, S., Thanarajan, T., Alotaibi, Y., Alghamdi, S., Brain Tumor: Hybrid Feature Extraction Based on UNet and 3DCNN (2023) *Computer Systems Science and Engineering*, 45 (2), pp. 2093-2109.

26. Ramesh, K.K.D., Kumar, G.K., Swapna, K., Datta, D., Rajest, S.S., A Review of Medical Image Segmentation Algorithms, AI Endorsed Transactions on Pervasive Health and Technology, 04 2021 - 06 2021, vol. 7, issue 27, e6
27. Schrauwen, B., Wandermann, M., Verstraeten, D., Steil, J.J., Stroobandt, D., Improving reservoirs using intrinsic plasticity, Neurocomputing, vol. 71, pp. 1159–1171 (2008)
28. Steil, J.J., Online reservoir adaptation by intrinsic plasticity for back-propagation-decoleration and echo state learning, Neural Networks, vol. 20, pp. 353–364 (2007)
29. Xu, M., Yoon, S., Fuentes, A., Park, D.S., A Comprehensive Survey of Image Augmentation Techniques for Deep Learning, Pattern Recognition, vol. 137, 2023, 109347.
30. Yadav, A.S., Kumar, S., Karetla, G.R., Cotrina-Aliaga, J.C., Arias-González, J.L., Kumar, V., Srivastava, S., Gupta, R., Ibrahim, S., Paul, R., Naik, N., Singla, B., Tatkar, N.S., A Feature Extraction Using Probabilistic Neural Network and BTFSC-Net Model with Deep Learning for Brain Tumor Classification (2023) Journal of Imaging, 9 (1), art. no. 10.
31. Yager, R., Filev, D., Generation of fuzzy rules by mountain clustering, Journal of Intelligent and Fuzzy Systems, vol. 2 (3), 1994, pp.209-219.
32. Zhang, H., Fritts, J.E., Goldman, S.A., Image segmentation evaluation: A survey of unsupervised methods, Computer Vision and Image Understanding, vol.110, 2008, pp.260–280
33. Zhang, H., Fritts, J.E., Goldman, S.A., An Entropy-based Objective Evaluation Method for Image Segmentation, Proceedings of SPIE - The International Society for Optical Engineering, January 2004, DOI: 10.1117/12.527167

**Petia Koprinkova-Hristova** is a Professor at the Institute of Information and Communication Technologies - Bulgarian Academy of Sciences, department of Parallel Algorithms and Machine Learning with Laboratory of Neurotechnologies. Her scientific interests are in the field of AI and particularly brain-inspired computing, neural networks and their applications in various fields such as brain functions modelling, reinforcement learning, optimization, image analyses etc.

**Ivan Georgiev** is an Associate Professor at the Institute of Information and Communication Technologies - Bulgarian Academy of Sciences - Head of Laboratory on 3D digitization and microstructural analysis. His scientific interests and experience are in the fields of: mathematical modeling and numerical simulations, biomedical, environmental and engineering applications. He is active also in the field of industrial computed tomography and microstructure analysis.

**Miryana Raykovska** is an Assistant at the Laboratory on 3D digitization and microstructural analysis, Institute of Information and Communication Technologies – Bulgarian Academy of Science. She has MSc degree in Endodontie. Her main research area is application of Micro-CT in the Medicine.

*Received: January 28, 2023; Accepted: June 20, 2023.*

